Oral presentation | Turbulence simulation (DNS,LES,RANS)
Turbulence simulation(DNS,LES,RANS)-III
Thu. Jul 18, 2024 10:45 AM - 12:45 PM Room B

[10-B-04] Numerical Simulation of Base Jet in Supersonic Flow with Gas-Kinetic Method

*Tao Liu[1], Qibing Li[1], Jianhui Wu[2], Yue Zhao[2] （1. Department of Engineering Mechanics, Tsinghua University, 2. China Academy of Launch Vehicle Technology）

Keywords: supersonic base jet, gas-kinetic scheme, multiscale scheme

Twelfth International Conference on Computational Fluid Dynamics (ICCFD12), Kobe, Japan, July 14-19, 2024

Numerical Simulation of Base Jet in Supersonic Flow with Gas-Kinetic Method

Tao Liu[a], Qibing Li[a,*], Jianhui Wu[b], Yue Zhao[b]
Corresponding author: lqb@tsinghua.edu.cn
[a] Department of Engineering Mechanics, Tsinghua University, China
[b] China Academy of Launch Vehicle Technology

Abstract: The interaction between the aircraft engine jet and the supersonic external flow is important to high-speed aircrafts, which involves complex flow phenomena such as supersonic turbulent boundary layer, jet and shock waves. The high fidelity simulation requires strong robustness and high accuracy of numerical methods. The gas-kinetic scheme combined with RANS model (RANS-GKS) is applied to get the large-scale mean fields of supersonic bottom jet flow. Then a multi-scale turbulence simulation method based on gas-kinetic scheme (MS-GKS) is applied to investigate the main characteristics. Both methods can obtain large-scale mean fields which agree well with experimental results. Besides, MS-GKS can capture small-scale structures and unsteady characteristics, such as the instability of the annular shear layer and vortex rolling up during the development of supersonic jet.
Keywords: Engine Jet, Supersonic External Flow, Gas-Kinetic Scheme, Multi-Scale Simulation Method.

1 Introduction

The interaction between the aircraft engine jet and the supersonic external flow has a significant impact on the forces and thermal environment in the base and wake regions. It involves complex flow structures such as supersonic boundary layer, expansion waves, shock waves, free shear layers, separated vortices and the mixing of jet and external flow.

A large amount of work has been done to study this supersonic base jet flow. Jackson et al. conducted an experimental study of the bottom jet interaction, and found that in the range of Mach 0.5 to 2.0, the jet has a great impact on the bottom resistance, but has no significant impact on the rest of the resistance[1]. Morris et al. experimentally studied the bottom jet under hypersonic freestream with Mach number 7.1, and various gas conditions[2]. Bannink et al. [3] carried out experiments on supersonic bottom jets with freestream Mach numbers 1.96 and 2.98 at different pressure ratios, and obtained detailed flow field data, providing the support for many numerical simulation works.

Bannink's group and Morris's group applied a variety of RANS models, such as S-A, k-ω and SST method to simulate the supersonic base jet flow. Two-dimensional axisymmetric (2D) and three-dimensional (3D) simulations are conducted. They found that, compared with laminal results, results of turbulence models agree better with the experimental data. The 3D results are obviously better than the 2D predictions.

Due to the large Reynolds number, the RANS method is commonly used to predict large-scale mean fields, which cannot capture small-scale structures and unsteady characteristics in the flow field. Besides the turbulence model, the strong robustness for simulating both supersonic external/jet flows and low-speed base flow, the high accuracy and high resolution to capture strong shock waves and small-scale vortices, as well as the instability of shear layers are all challenging for a numerical method.

In recent years, the gas-kinetic scheme (GKS)[4] has increasingly demonstrated its unique advantages in high-speed complex flow. GKS automatically couples viscous and non-viscous effects, effectively balancing high accuracy and strong robustness in high-speed flow.

In this study, the RANS-GKS coupled with the S-A turbulence model is applied to simulate the supersonic base jet flow[10]. Then the multiscale scheme (MS-GKS) [5]is adopted to investigate the fine structures and unsteady evolution characteristics of the interaction of base jet and supersonic external flow.

2 Numerical Methods

2.1 Gas-Kinetic Scheme

The gas-kinetic scheme describes flow by solving the BGK-Boltzmann equation within the finite volume. The 3D BGK-Boltzmann equation is written as

$$\frac{\partial f}{\partial t}+\mathbf{u}\cdot\nabla f=\frac{g-f}{\tau} \tag{1}$$

Among them, f is the mesoscopic gas distribution function, and τ is the relaxation time of molecular motion. g is the equilibrium distribution, and f and g are functions of high-dimensional phase space, namely space $\mathbf{x}$, time t, velocity $\mathbf{u}$, and internal degrees of freedom ξ. In general, it can be assumed that g is the Maxwellian distribution function, which can be uniquely determined by macroscopic conservation quantities $\mathbf{W}=(\rho,\rho\mathbf{U},\rho E)^T$:

$$g=\rho\left(\frac{\lambda}{\pi}\right)^{\frac{K+3}{2}}\mathrm{e}^{-\lambda((\mathbf{u}-\mathbf{U})^2+\xi^2)} \tag{2}$$

where ρ is density, p is pressure, E is energy density, $\lambda=\rho/(2p)$,
$\xi^2=\xi_1^2+\xi_2^2+\cdots+\xi_K^2$, K is the number of internal degrees of freedom, and in the three-dimensional format, $K=2$.

The equation has a general solution,

$$f(\mathbf{x},t,\mathbf{u},\xi)=\frac{1}{\tau}\int_0^t g(\mathbf{x}',t',\mathbf{u},\xi)\mathrm{e}^{-(t-t')/\tau}\mathrm{d}t'+\mathrm{e}^{-t/\tau}f_0(\mathbf{x}-\mathbf{u}t,\mathbf{u},\xi) \tag{3}$$

and the f_0 is initial gas distribution function. After getting the distribution function, the macroscopic quantity and the fluxes at the grid interface can be obtained through integration over the velocity and internal freedom space,

$$\mathbf{W}=(\rho,\rho\mathbf{U},\rho E)^T=\int f\boldsymbol{\psi}\mathrm{d}\Xi \tag{4}$$

$$\mathbf{F}_i=\int u_i f\boldsymbol{\psi}\mathrm{d}\Xi, i=1,2,3 \tag{5}$$

where $\boldsymbol{\psi}=(1,\mathbf{u},\frac{1}{2}(\mathbf{u}^2+\xi^2))^T$, $\mathrm{d}\Xi=\mathrm{d}u_1\mathrm{d}u_2\mathrm{d}u_3\mathrm{d}\xi_1\cdots\mathrm{d}\xi_K$。

The macroscopic conservation quantities within grid elements in GKS are updated using the finite volume method：

$$\mathbf{W}_{i,j,k}^{n+1}=\mathbf{W}_{i,j,k}^{n}+\frac{1}{\Omega_{i,j,k}}\sum_m \Delta S_m\int_0^{\Delta t}\int u_m\hat{f}_m(t,u,\xi)\boldsymbol{\psi}\mathrm{d}\Xi\mathrm{d}t \tag{6}$$

For specific details, please refer to [4].

2.2 Extended GKS for Turbulence Simulation

To simulate high Reynolds number turbulence flow, the BGK equation can be extended to establish an extended GKS by introducing turbulence models. In turbulence research, velocity can generally be decomposed into the average velocity and the fluctuation. In the Boussinesq hypothesis, the effect of small-scale fluctuations on the large-scale mean field is similar to that of microscopic molecular processes[6]. Therefore, the effect of turbulent fluctuations on the mean flow field can be described by defining the turbulent viscosity coefficient. Under this assumption, the relaxation process of molecular thermal motion and turbulent fluctuation can be uniformly described by the extended BGK equation, that is, the relaxation process of gas molecules from microscopic thermal motion to macroscopic turbulent mean field:

$$\frac{\partial f}{\partial t} + \mathbf{u} \cdot \nabla f = \frac{g - f}{\tau_e} \tag{7}$$

The distribution function in the above equation *f* is still a distribution function in phase space, and the difference from the original BGK equation is that the large-scale *g* is defined on the scale of the turbulent mean field, so the relevant parameters in the Maxwellian distribution are related to the large-scale mean flow field. The effective relaxation time is defined as:

$$\tau_e = \frac{\mu + \mu_t}{p + 2k/3} \tag{8}$$

Where μ and p are the molecular viscosity coefficient and flow field pressure, and k is the turbulent kinetic energy of the flow field. In addition, when updating the total energy, the contribution of turbulent kinetic energy should be considered. When the Mach number in the flow field is not very large ($\leqslant 5$), the influence of k can usually be ignored. μ_t and k can be obtained by solving the turbulence model equation, and the transport of turbulent flow can be coupled and solved through the GKS with scalar transport[7], thereby ensuring high solution accuracy. Through turbulent viscosity, turbulence models can be directly combined with GKS schemes to develop methods such as RANS-GKS, GKS-DES, and GKS-IDDES.

2.3 Multi-Scale GKS for Turbulence Simulation

For GKS-DES and GKS-IDDES, the multi-scale characteristics come from the turbulence model itself, while the multi-scale characteristics of the MS-GKS method come from the multi-scale characteristics of GKS itself.

On the basis of the GKS format, the MS-GKS method reconstructs the velocity distribution function and turbulence characteristic time. The initial gas distribution function f_0 is used to describe small-scale turbulence fluctuations, and the LES model is used for modeling. Simultaneously, the equilibrium distribution function g is used to describe the average field of large-scale turbulence, and the RANS model is used for modeling. Based on the relaxation process of f_0 to g in the BGK model equation, MS-GKS achieves smooth switching between different scales. In the present study, the S-A turbulence model is applied for RANS [10] and the Vreman's model chosen for LES [11].

MS-GKS assumes that the relaxation process of turbulent fluctuation at different scales satisfies the extended BGK equation. In this description, turbulent fluctuation is directly analogized to molecular thermal motion. Through the extended BGK equation, the relaxation process of molecular thermal motion and turbulent fluctuation can be uniformly described, that is, the relaxation process of gas molecules from microscopic thermal motion to macroscopic turbulent mean field. The general solution of the extended BGK equation is

$$f(\mathbf{x},t,\mathbf{u},\xi)=\frac{1}{\tau_e}\int_0^t g(\mathbf{x}-\mathbf{u}t',t',\mathbf{u},\xi)\mathrm{e}^{-(t-t')/\tau_e}\mathrm{d}t'+\mathrm{e}^{-t/\tau_e}f_0(\mathbf{x}-\mathbf{u}t,\mathbf{u},\xi) \tag{9}$$

By combining the Taylor expansion in space and time, the gas distribution function at the grid interface ***x=0*** can be obtained:

$$\begin{aligned}
f=&(1-C_0^e)\,g_0+(t-\tau+C_1^{e,1})\,\bar{A}g_0\\
&+(-\tau+C_1^{e,1}+C_2^e)(\bar{a}_m^l u_m H[u_1]+\bar{a}_m^r u_m(1-H[u_1]))\,g_0\\
&+(C_0^e-(C_1^{e,1}+C_2^e)\,a_m^l u_m-C_1^{e,1}A^l)H[u_1]g^l\\
&+(C_0^e-(C_1^{e,1}+C_2^e)\,a_m^r u_m-C_1^{e,1}A^r)(1-H[u_1])\,g^r\\
&-(1-C_0^e)\,\tau_t(\bar{a}_m^l u_m H[u_1]+\bar{a}_m^r u_m(1-H[u_1])+\bar{A})\,g_0\\
&-C_0^e\tau_t((a_m^l u_m+A^l)H[u_1]g^l+(a_m^r u_m+A^r)(1-H[u_1])\,g^r)
\end{aligned} \tag{10}$$

$$\tau_e=\tau+\tau_t,C_0^e=\mathrm{e}^{\frac{-t}{\tau_e}},C_1^e=\tau_e C_0^e,C_2^e=tC_0^e,C_1^{e,1}=\tau C_0^e \tag{11}$$

Except for the last two items, the forms of the other items are consistent with the GKS format, with the only difference being that they mainly affect the numerical dissipation characteristics C_0^e and $C_1^{e,1}$,Therefore, if it can be made consistent with the GKS format, the first five terms are at the NS scale. For the latter two items, f_0 constructed at the LES scale and g the RANS scale respectively, then multi-scale characteristics are introduced. The above equation can be simply written as

$$f(\mathbf{0},t,\mathbf{u},\xi)=f^{NS}+H_R(\mathcal{T})f^{neq,R}+H_L(\mathcal{T})f^{neq,L} \tag{12}$$

The superscripts R, L, and NS represent RANS, LES, and NS scales, respectively.

From the above equation, when the non-equilibrium term of turbulence, i.e. the last two terms, is zero, the distribution function approaches the NS scale. When the last two terms are not zero, the scale of the distribution function can be controlled by H_L and H_R, which will be affected by the time scale function $\mathcal{T}$. Therefore, the key of MS-GKS is to model the time scale function $\mathcal{T}$.

Considering that most existing turbulence models are based on the characteristic length scale, MS-GKS assumes that the ratio of turbulence characteristic time to characteristic length at different scales is linear. Further considering the anisotropy of flow field and maintaining the simulation ability of Vreman-LES model for transition, the final model is as follows:

$$\mathcal{T}_i=C_{MS}\frac{F_{LW}}{F_{RW}}\left(\frac{l_R}{l_L}+\frac{\Delta_i^2}{\Sigma_j\Delta_j^2}(\chi_{i,in}^2+\chi_{i,out}^4)\right) \tag{13}$$

where the l_R is the length scale of RANS model, l_L is the length scale of LES model, Δ_i is the local length scale of computational cell in the i direction, $\chi_{i,in}^2$ and $\chi_{i,out}^4$ enable the switch of MS-GKS to LES scale quickly when the mesh is fine.C_{MS} is a model parameter which depends on the specific RANS model and LES model. For specific details, please refer to [5].

MS-GKS provides a computational framework that can couple turbulence models at different scales, which includes the contribution of adopted RANS and LES models, the local flow characteristics, and the local length scale of computational cells. The change of modeling scale is controlled by the relaxation mechanism of BGK equation. It is not necessary to directly model the function corresponding to the relaxation process, nor to manually partition the traditional RANS-LES hybrid method. MS-GKS explicitly includes turbulence models on RANS and LES scales, which can return to these two models at the limit of flow field resolution. In addition, the BGK relaxation mechanism and its cross-scale evolution solution have clear

and universal physical meaning, based on which the constructed MS-GKS is simple and has good universality. Although the current LES and RANS models in MS-GKS are based on the eddy viscosity assumption, in fact, other turbulence models can also be adopted.

3 Numerical Results and Discussion

3.1 RANS simulation

In the current study, typical base jets in supersonic flow are simulated. The length of the aircraft model is $L=186.81\,\mathrm{mm}$, the diameter of the bottom is $D=50\,\mathrm{mm}$, as well as the diameter of the jet outlet $d=17\,\mathrm{mm}$. More details can be found in [1].

Tables 1 and 2 show the specific parameters of the bottom jet at freestream Mach numbers $\mathrm{Ma}_\infty=1.96$ and $\mathrm{Ma}_\infty=2.98$. p_∞ is the static pressure of the freestream, $T_{t,\infty}$ is the total temperature of the freestream, and Re_L is the freestream Reynolds number based on the model length L. p_{t_j} and T_{t_j} are the total pressure and temperature of the jet, respectively. α is the angle of attack. The size of computational domain is 400mm in the streamwise direction and 150mm in the radial direction. Different combustion chamber pressure ratios and attack angles are computed, as well as an additional case without jet for comparison.

The far-field conditions based on the local one-dimensional Riemann invariants are adopted at the outer boundary. For the absence of jet flow, the left boundary of nozzle is a no-slip and adiabatic solid wall. For the case of jet flow, the boundary conditions are given based on the total temperature and pressure. All other walls are no-slip and adiabatic solid wall.

As mentioned in [8], the number of grid cells in the bottom region has a significant impact on the flow, so a certain degree of grid refinement in the bottom region is necessary. Therefore, in the present study, different computational cell numbers are considered from 3 million to 25 million, mainly by increasing the number in the bottom region. It is found that when the numbers reach about 6 million, the predicted bottom pressure by these grids are almost the same. The normal length of the first layer grid is 1.0×10^{-3} mm.

Table 1 Parameters of the base jet, freestream Mach number 1.96

$\mathrm{Ma}_\infty=1.96, p_\infty=0.0283\,\mathrm{MPa}, T_{t,\infty}=285\,\mathrm{K}, \mathrm{Re}_L=5.16\times10^6$			
p_{t_j} (MPa)	T_{t_j} (K)	$N=p_{t_j}/p_\infty$	$\alpha(^\circ)$
4.92	287	173.9	0
9.90	287	349.5	0
9.90	287	349.5	10

Table 2 Parameters of the base jet, freestream Mach number 2.98

$\mathrm{Ma}_\infty = 2.98, p_\infty = 0.01616\,\mathrm{MPa}, T_{t,\infty} = 285\,\mathrm{K}, \mathrm{Re}_L = 8.70\times10^6$			
p_{t_j} (MPa)	T_{t_j} (K)	$N = p_{t_j}/p_\infty$	α(°)
3.13	287	193.5	0
9.89	287	612.1	0
9.89	287	612.1	10

Figure 1 shows the pressure distribution on the side wall under different conditions. The simulated results are in good agreement with the experiment. Figure 2 shows the distribution of bottom pressure, compared with the results obtained by 3D RANS simulation in [9]. In the absence of jet flow, the deviation between the present numerical results and experimental measurements is small, which is basically consistent with the results obtained by other RANS methods. In the case of jet flow, the deviation from the experimental data is also relatively small, which is significantly better than existing RANS results in [9].

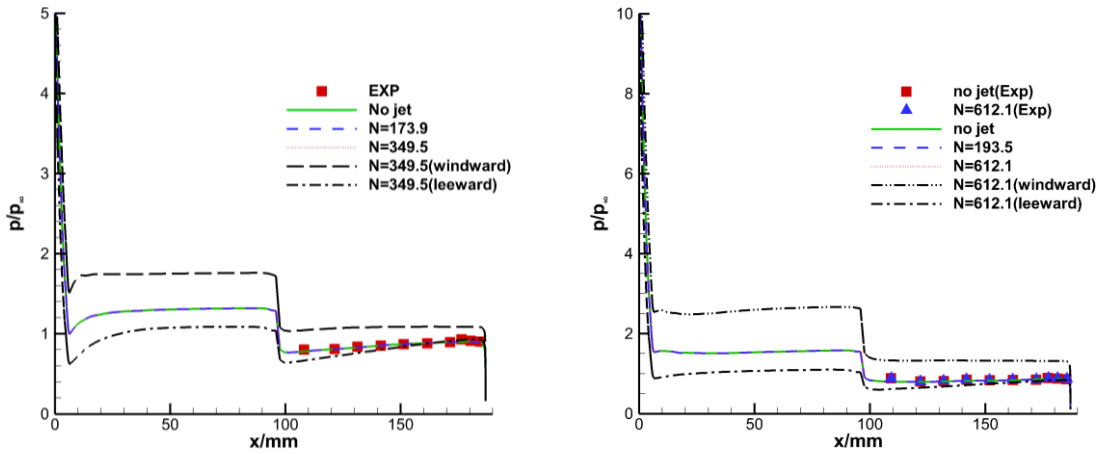

Figure 1 Pressure distribution on the side wall (left: $\mathrm{Ma}_\infty = 1.96$; right: $\mathrm{Ma}_\infty = 2.98$)

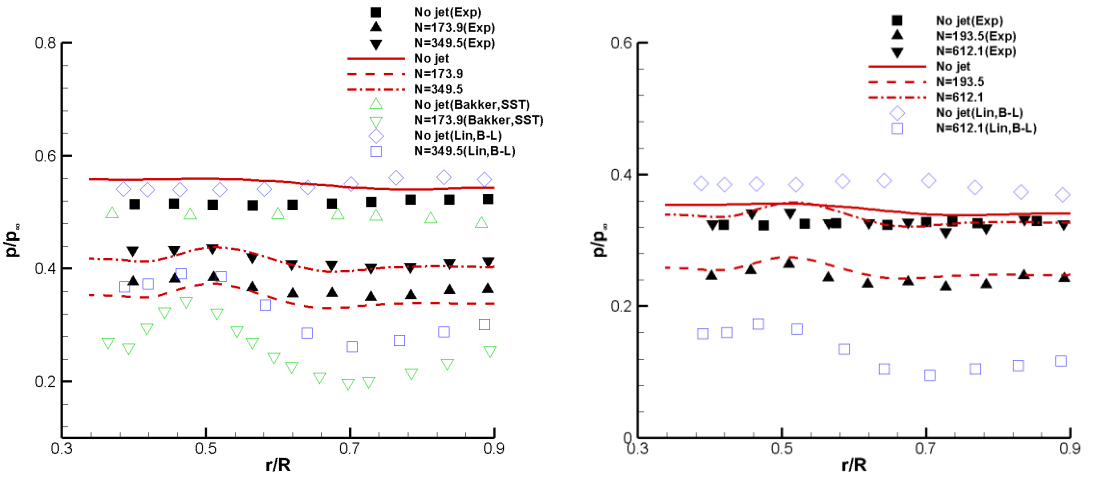

Figure 2 Pressure distribution on the bottom (left: $\mathrm{Ma}_\infty = 1.96$; right: $\mathrm{Ma}_\infty = 2.98$)

Figure 3 shows the simulated Mach number contours for different freestream Mach number and jet pressure ratio. The free shear layers, different shock waves, expansion waves and vortex structures can be clearly observed. Figure 4 and Figure 5 show the effect of jet on the flow fields. Compared with the flow without a jet, the flow structure in the bottom region changes significantly. The high temperature and low Mach number in the nozzle and the outlet are replaced by lower temperature and higher Mach number due to the expansion of gas from the combustion chamber.

Figure 6 shows the streamlines with different freestream angles of attack. In both cases, there is a dominant large vortex in the bottom region, along with some small vortices. The shape and size of vortices vary significantly due to the freestream angle of attack which affect the aerodynamic forces and thermal environment of the aircraft.

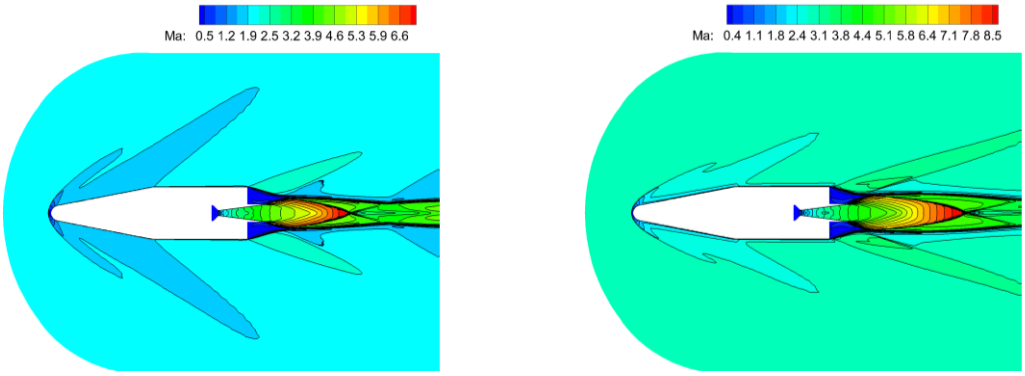

Figure 3 Mach number contours (left: freestream Mach number 1.96, pressure ratio 349.5; right: freestream Mach number 2.98, pressure ratio 612.1)

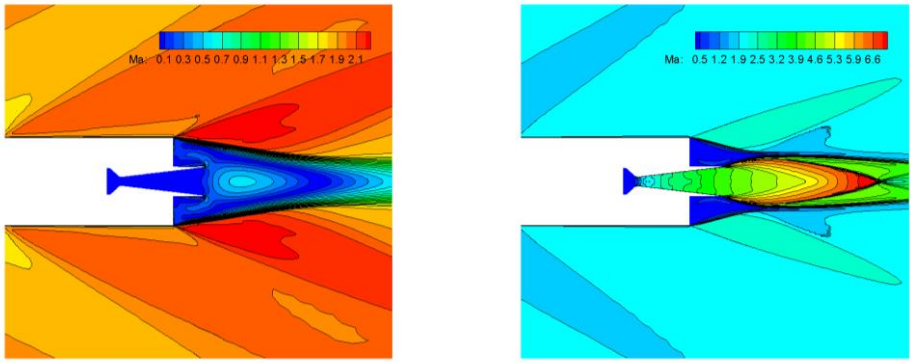

Figure 4 Mach number contours, freestream Mach number 1.96 (left: no jet; right: pressure ratio 349.5)

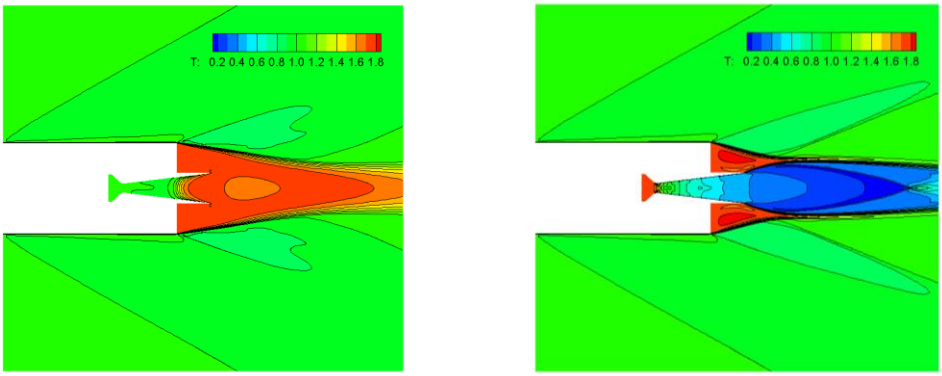

Figure 5 Temperature contours, freestream Mach number 1.96 (left: no jet; right: pressure ratio 349.5)

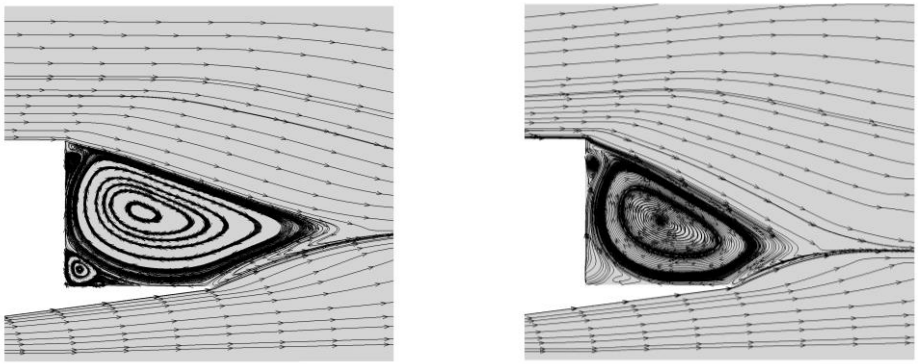

Figure 6 Streamlines in the bottom region for, freestream Mach number 1.96 (left: no attack; right: $\alpha = 10°$)

3.2 Multiscale simulation

In the above-mentioned simulation, RANS-GKS predicted flow characteristics such as bottom pressure are in good agreement with the experiment. However, RANS simulation can only give large-scale mean fields and cannot capture small-scale structures and unsteady characteristics in the flow field. To obtain more fine flow structures, we conduct fine simulations using MS-GKS. For better resolving the unsteady development of jet, larger computational domain is adopted in the streamwise direction.

Furthermore, MS-GKS is used to simulate the base jet in supersonic flow under different conditions. The specific parameters are shown in Table 3. The size of computational domain is 1200mm in the streamwise direction and 150mm in the radial direction. Approximately 16.5 million grid cells are adopted. RANS-GKS is applied to provide an initial field. Implicit scheme based on LU-SGS is applied in MS-GKS, thus the time step is chosen as about $0.0035 d/U_\infty$. The maximum number for inner iteration is 20 and the statistical duration for mean flow is about $58 d/U_\infty$.

Table 3 Parameters table of the base jet, freestream Mach number 1.96

$\mathrm{Ma}_\infty = 1.96, p_\infty = 0.0283\,\mathrm{MPa}, T_{t,\infty} = 285\,\mathrm{K}, \mathrm{Re}_L = 5.16 \times 10^6$			
p_{t_j} (MPa)	T_{t_j} (K)	$N = p_{t_j}/p_\infty$	$\alpha(°)$
4.92	287	173.9	0
9.90	287	349.5	0
9.90	287	349.5	10

Figure 7 shows the mean pressure and temperature distribution on the side wall of the aircraft model. As the unsteady characteristics of forebody region are not strong, the predicted side-wall pressure by MS-GKS is almost the same as that by RANS-GKS, and both of them are in good agreement with the experiment. The side-wall temperature predicted by MS-GKS shows only a little difference when compared with RANS-GKS result.

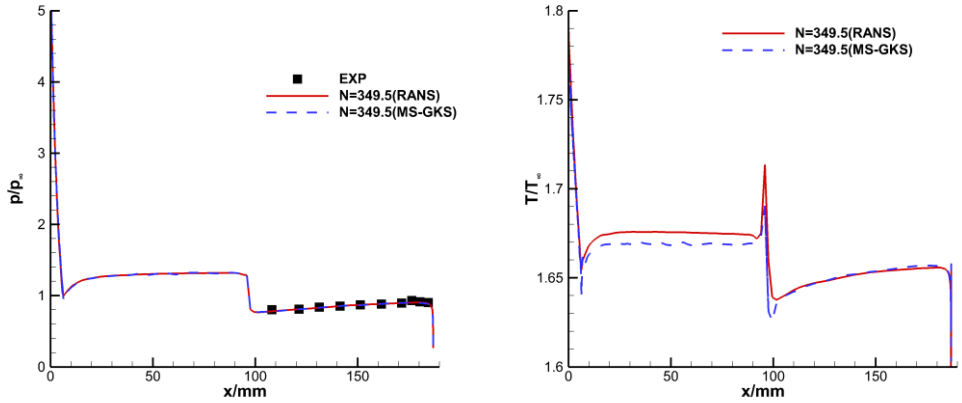

Figure 7 Mean pressure and temperature distribution on the side wall, freestream Mach number 1.96, pressure ratio 349.5 (left: pressure; right: temperature)

Figure 8 shows the instantaneous Mach number contours under different conditions. Compared with the RANS results, MS-GKS can capture the process of boundary layer instability and vortex roll-up in the wake region. Due to the larger grid scale in the downstream, the small-scale structure gradually disappears. For different freestream Mach numbers, as the pressure ratio of the nozzle combustion chamber increases, the position of the shock wave intersection changes, and it moves further away from the nozzle outlet. The interaction between the jet and the external flow causes shear layer instability in a certain area away from the bottom, with continuous vortices rolling up. In the case of nonzero angle of attack, the symmetry of the shear layer is disrupted, one side of the layer instability is suppressed, and the structure of the Mach disk also changes.

Figure 9 shows the instantaneous vortex structures identified by the Q criterion under different conditions. There are vortices near the bottom of the aircraft model and vortices moving downstream in a spiral motion. Inside the annular mixing layer, the flow contraction and expansion, and the Mach disk can also be observed. For the case with zero angle of attack, the instantaneous vortex structures exhibit spiral horizontal backward motion characteristics and a certain degree of symmetry. For the case with an angle of attack, it shows a situation where one side has fewer vortices and the other side has more vortices.

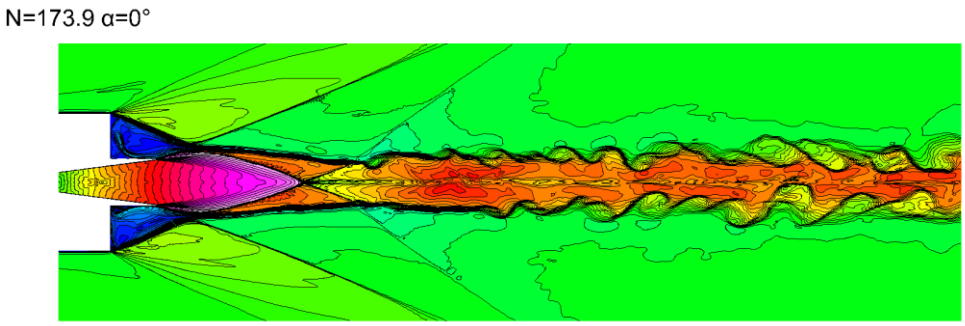

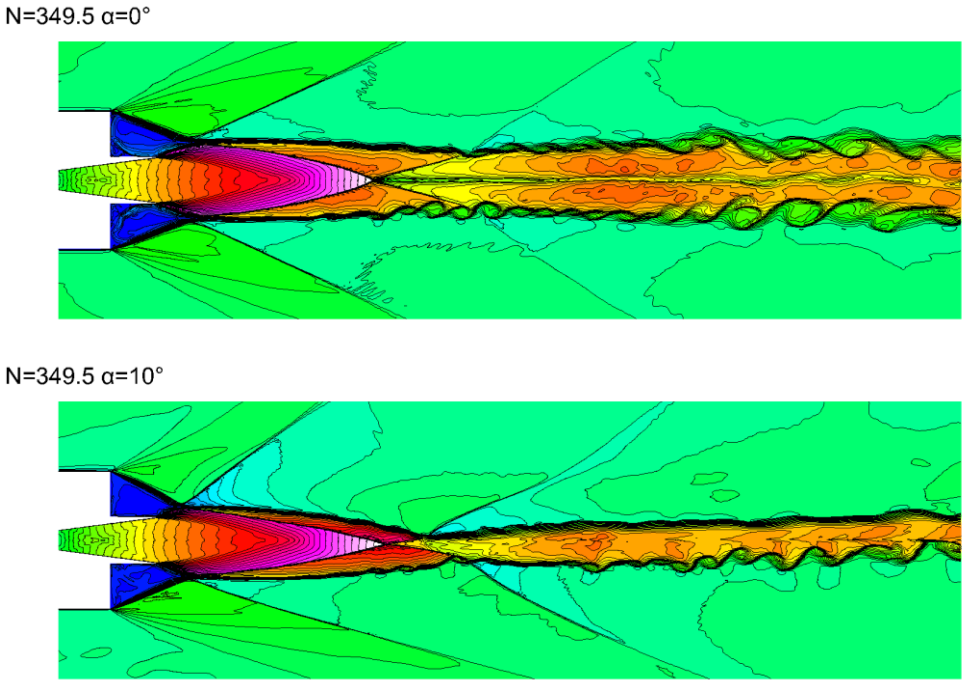

Figure 8 Instantaneous contours of the Mach number near the bottom, $\mathrm{Ma}_\infty = 1.96$

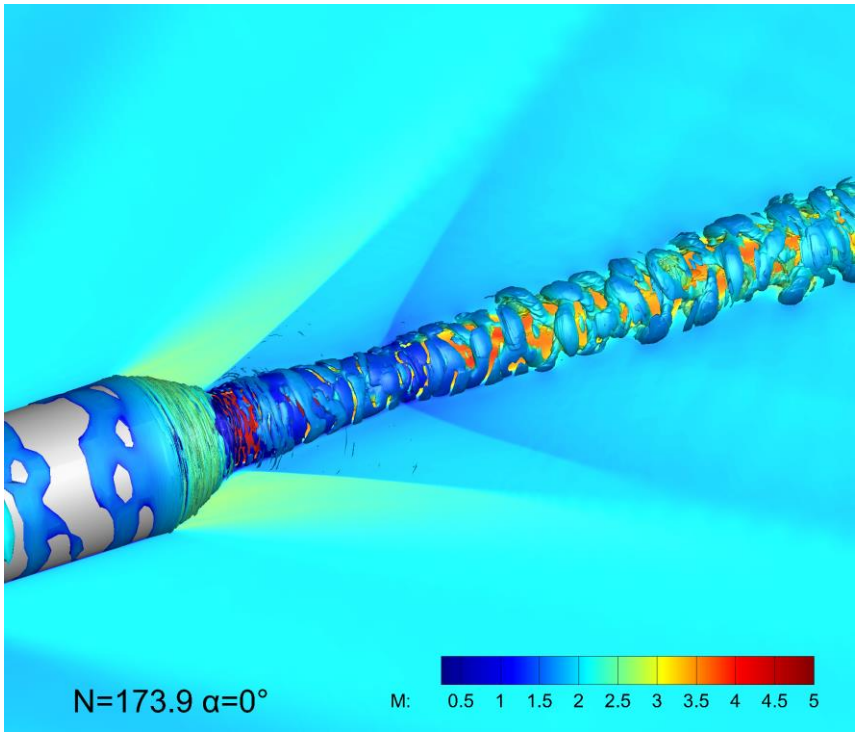

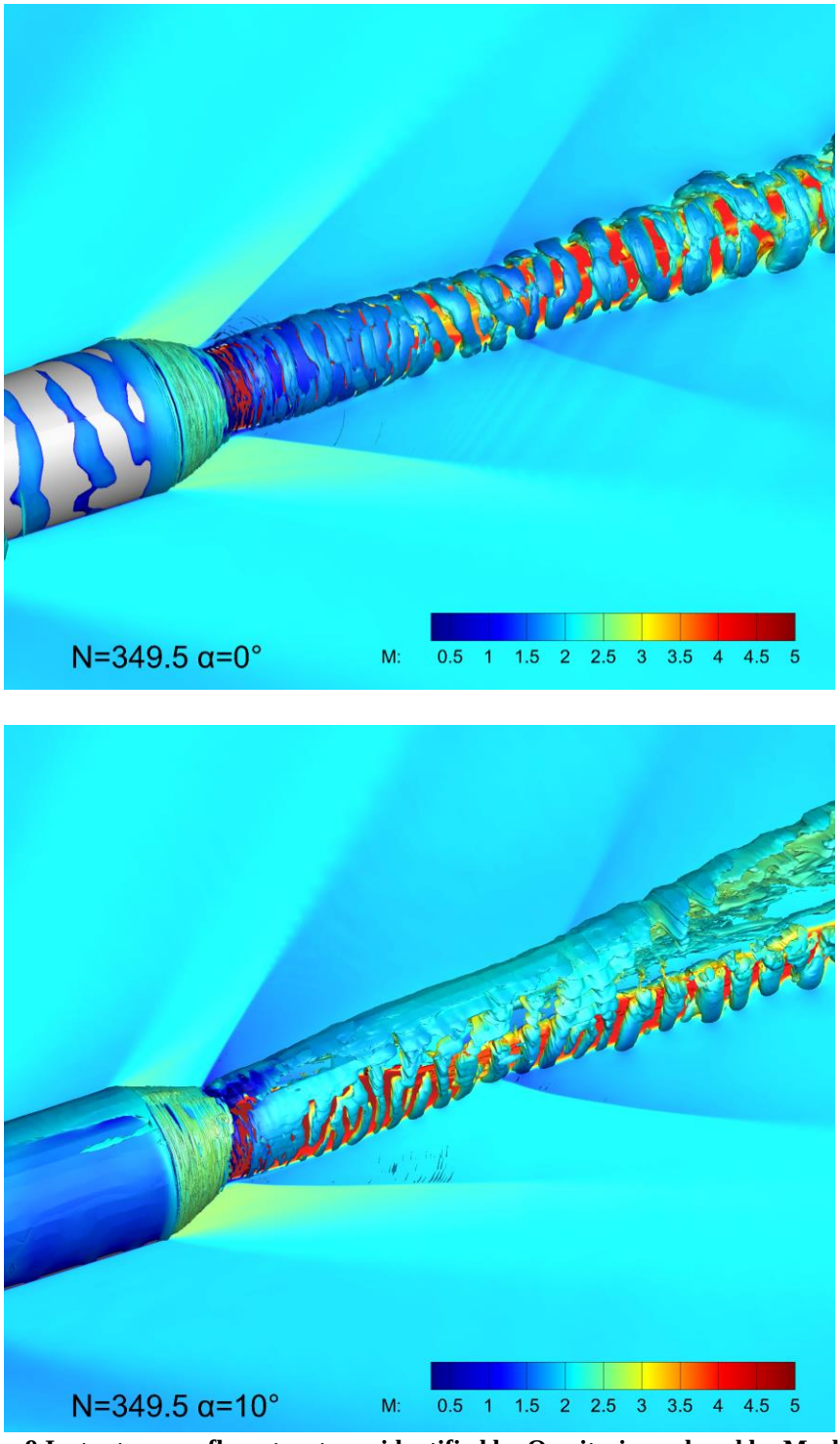

Figure 9 Instantaneous flow structures identified by Q-criterion colored by Mach number, $\mathrm{Ma}_\infty = 1.96$ (nondimensional Q=100)

3 Conclusions

The supersonic base jet flow is numerically investigated using two gas-kinetic schemes for turbulence simulations: RANS-GKS for large-scale mean flow fields, and MS-GKS for multi-scale structure capturing. Both methods can obtain mean fields which agree well with experimental results. Besides, MS-GKS can capture small-scale structures and unsteady characteristics, such as the instability of the annular shear layer and vortex rolling up during

the development of supersonic jet. The effects of freestream Mach number, angle of attack and nozzle pressure ratio are discussed. The present study shows the good performance the GKS method for high-Reynolds number flows when combined with turbulence models.

Acknowledgements

This work is supported by the National Natural Science Foundation of China (Nos. 11672158 and 12388101) and the National Key Project (No. GJXM92579).

References

[1] H.H Jackson. Longitudinal aerodynamic characteristics and effect of rocket jet on drag of models of the Hermes A-3A and A-3B missiles in free flight at Mach numbers from 0.6 to 2.0. Technical Report Archive & Image Library. 1955.
[2] N. Morris, D. Buttsworth, T. Jones. An experimental and computational study of moderately underexpanded rocket exhaust plumes in a co-flowing hypersonic free stream. East Afr. Med. J. 1995
[3] W.J. Bannink, E. Houtman, P. Bakker. Base flow/underexpanded exhaust plume interaction in a supersonic external flow. 8th AIAA International Space Planes and Hypersonic Systems and Technologies Conference. 1998.
[4] K. Xu. A gas-kinetic BGK scheme for the Navier–Stokes equations and its connection with artificial dissipation and Godunov method. J. Comput. Phys. 2001, 171(1):289-335.
[5] S. Tan, Q.B. Li, S. Fu. A multiscale gas-kinetic scheme for turbulence simulation. 6th symposium on Hybrid RANS-LES Methods(HRLM6). Strasbourg, France, 2016.
[6] H. Chen, S. Kandasamy, S. Orszag, et al. Extended Boltzmann kinetic equation for turbulent flows. Science. 2003, 301(5633): 633-636
[7] Q.B. Li, S. Fu, and K. Xu. A compressible Navier–Stokes flow solver with scalar transport. J. Comput. Phys. 2005, 204 (2005):692-714.
[8] J.Z. Lin, H. Li, X.Q. Fang, et al. Numerical simulation of supersonic base jet interference flow field. Acta Aerodyn. Sin. 2005,23(4), 516-520
[9] P.G. Bakker, et al. CFD validation for base flows with and without plume interaction. AIAA paper. 2002, 2002-0438.
[10]P. R. Spalart. A one-equation turbulence model for aerodynamic flows. AIAA J. 1992.
[11]A. W. Vreman. An eddy-viscosity subgrid-scale model for turbulent shear flow: Algebraic theory and applications. Phys. Fluids. 2004, 16(10):3670-3681.